

# The obscuration by dust of most of the growth of supermassive black holes

Alejo Martínez-Sansigre<sup>†</sup>, Steve Rawlings<sup>†</sup>, Mark Lacy<sup>‡</sup>, Dario Fadda<sup>‡</sup>, Francine R. Marleau<sup>‡</sup>, Chris Simpson<sup>\*</sup>, Chris J. Willott<sup>◊</sup>, Matt J. Jarvis<sup>†</sup>

<sup>†</sup>Astrophysics, Department of Physics, University of Oxford, Keble Road, Oxford OX1 3RH, UK

<sup>‡</sup>Spitzer Science Center, California Institute of Technology, MS220-6, 1200 E. California Boulevard, Pasadena, CA 91125, USA

<sup>\*</sup>Department of Physics, University of Durham, South Road, Durham DH1 3LE, UK

<sup>◊</sup>Herzberg Institute of Astrophysics, National Research Council, 5071 West Saanich Rd, Victoria, B.C. V9E 2E7, Canada

---

Supermassive black holes underwent periods of exponential growth during which we see them as quasars in the distant Universe. The summed emission from these quasars generates the cosmic X-ray background, the spectrum of which has been used to argue that most black-hole growth is obscured<sup>[1–2]</sup>. There are clear examples of obscured black-hole growth in the form of ‘type-2’ quasars<sup>[3–5]</sup>, but their numbers are fewer than expected from modelling of the X-ray background. Here we report on the direct detection of a population of distant type-2 quasars which is at least comparable in size to the well-known unobscured type-1 population. We selected objects that have mid-infrared and radio emissions characteristic of quasars, but which are faint at near-infrared and optical wavelengths. This population is responsible for most of the black hole growth in the young Universe and, throughout cosmic history, black-hole growth occurs in the dusty, gas-rich centres of active galaxies.

---

The population of unobscured type-1 quasars is now well understood out to redshift  $z \sim 2$  by virtue of optical surveys<sup>[6]</sup> which provide direct measurements around the “break” in the luminosity function where the quasar population outputs most of its luminosity density. Current understanding of the obscured type-2 quasar population is far less complete.

Examples of type-2 quasars have, for many years, been confined mainly to radio-selected samples. Radio emission is unaffected by dust and, at low frequencies, is not strongly dependent on viewing angle so the simplest interpretation of optical spectroscopic follow-up of

radio-selected samples is that luminous quasars divide roughly equally into obscured (type-2) and unobscured (type-1) objects<sup>[7]</sup>. However, ‘radio-loud’ quasars are rare and may be atypical: their large-scale radio jets may well modify their environments in ways which influence whether or not the nucleus is obscured, and hence the ratio of quasars in the type-1 and type-2 classes<sup>[8]</sup>.

More recently, deep X-ray surveys and optical surveys have also been successful in identifying type-2 quasars<sup>[5,9,10]</sup>. However, optical spectroscopic follow-up has yet to find a type-2 population which can account fully for the X-ray background<sup>[1,9,11]</sup>. This is believed to be because a substantial fraction of type-2 quasar nuclei are hidden by ‘Compton thick’ material (with neutral gas column densities  $N_H \gtrsim 10^{28} \text{ m}^{-2}$ ) even when observed at high X-ray energies<sup>[1,12]</sup>.

type-2 quasars (with visual extinction  $A_V \gtrsim 5$  magnitudes towards their nuclei) fail to outshine their host galaxy at ultra-violet and optical wavelengths. However, at longer wavelengths the obscuration becomes small so the mid-infrared to radio properties of type-2 quasars should be similar to those of their type-1 counterparts, unless the obscuration or redshift becomes extreme. Indeed a survey at 60  $\mu\text{m}$  with the Infrared Astronomy Satellite (IRAS) led to the discovery of the first high-redshift radio-quiet type-2 quasar: the  $z = 2.3$  galaxy IRAS F10214+4724<sup>[4]</sup>. However, this object was discovered only because its flux was magnified by a factor  $\sim 50$  by a gravitational lens<sup>[13]</sup>. From the presence of high-excitation narrow lines and scattered broad lines<sup>[14]</sup> it clearly has an obscured type-2 nucleus but its X-ray emission seems to be obscured by Compton-thick material<sup>[12]</sup>.

With the advent of the Spitzer Space Telescope<sup>[15]</sup>, with a sensitivity  $\gtrsim 100$  times greater than IRAS and  $\gtrsim 10$  than the Infrared Space Observatory (ISO), type-2 quasars similar to IRAS F10214+4724 can be found from their mid-infrared emission without the aid of gravitational lenses. We chose the following selection criteria to find high-redshift type-2 quasars in the Spitzer First Look Survey (FLS): mid-infrared 24- $\mu\text{m}$  flux density  $S_{24\mu\text{m}} > 300 \mu\text{Jy}$ ; near-infrared 3.6- $\mu\text{m}$  flux density  $S_{3.6\mu\text{m}} \leq 45 \mu\text{Jy}$ ; and  $350 \mu\text{Jy} \leq S_{1.4\text{GHz}} \leq 2 \text{ mJy}$ , where  $S_{1.4\text{GHz}}$  is the 1.4-GHz radio flux density.

The mid-infrared ( $S_{24\mu\text{m}}$ ) criterion was chosen to obtain a reliable ( $7\sigma$ ) catalogue from the Spitzer FLS data from the MIPS instrument (Fadda, D., *et al.*, in preparation). At  $z = 2$  this means the quasar luminosity will be  $\gtrsim 0.2 L_{\text{quasar}}^*$  (where  $L_{\text{quasar}}^*$  is the break luminosity which corresponds to  $M_B = -25.7$  magnitudes<sup>[16]</sup>); this means we can detect sources around the break in the luminosity function (see Supplementary Information). Observed 24  $\mu\text{m}$

corresponds to emitted  $8 \mu\text{m}$  at  $z = 2$ , and dust extinction is negligible at this wavelength unless the obscuring column is extreme. (We adopt a  $\Lambda\text{CDM}$  cosmology with the following parameters:  $h = H_0/(100 \text{ km s}^{-1} \text{ Mpc}^{-1}) = 0.7$ ;  $\Omega_m = 0.3$ ;  $\Omega_\Lambda = 0.7$ .)

The upper limit on the  $3.6 \mu\text{m}$  flux density (obtained using the IRAC instrument<sup>[17]</sup>) was chosen to select only the most distant type-2 quasars. At  $z \geq 2$  the detected  $3.6\text{-}\mu\text{m}$  flux density corresponds to light emitted at  $\lambda \leq 1.2 \mu\text{m}$ , so we are able to eliminate unobscured, type-1 quasars whose flux would exceed this limit (FIG 1). Indeed, for type-2 quasars the  $S_{3.6\mu\text{m}}$  emission is likely to be dominated by starlight from the host galaxy, allowing us to estimate ‘photometric redshifts’  $z_{\text{phot}}$  (see Supplementary Information). Our  $S_{3.6\mu\text{m}}$  criterion corresponds to  $z_{\text{phot}} \gtrsim 1.4$  (see caption to Table 1 for more details).

The  $S_{3.6\mu\text{m}}$  criterion includes objects without IRAC detections which we expect to have the highest redshifts. Since the  $24\text{-}\mu\text{m}$  positions are accurate to  $\sim 1 \text{ arcsec}$ , the FLS radio positions<sup>[18]</sup>, accurate to  $\sim 0.5 \text{ arcsec}$ , were better for spectroscopic follow-up. However, the main importance of the radio selection criteria is to ensure that the candidates are quasars rather than starburst galaxies. We chose a lower limit on  $S_{1.4\text{GHz}}$  well above the level reached by high-redshift (submillimetre-selected) starburst galaxies without the benefit of gravitational lensing<sup>[19]</sup> and an upper limit to filter out the radio-loud objects, whose extended jets might complicate interpretation.

FIG. 1 shows the location of the 21 type-2 quasar candidates that met our selection criteria in the  $S_{24\mu\text{m}}$  versus  $S_{3.6\mu\text{m}}$  plane and Table 1 summarises their properties. The candidates were found from a sky area of  $3.8 \text{ deg}^2$  in the Spitzer FLS. No type-1 quasar ( $A_V = 0$ ) that is bright enough to be detected at  $24 \mu\text{m}$  will be faint enough at  $3.6 \mu\text{m}$  to be selected (FIG. 1). ‘Blind’ low-resolution optical spectroscopy<sup>[20]</sup> was performed on our 21 candidates, 10 of which yielded clear type-2 spectra with narrow emission lines giving redshifts in the range  $1.4 \lesssim z \lesssim 4.2$ . These objects are clearly type-2 quasars either because they have high-excitation lines (e.g. inset to FIG. 1) or because the rest-frame equivalent widths of their Ly- $\alpha$  lines are  $> 100 \text{ nm}$  and hence significantly larger than those seen in starbursts. Of the 11 objects that yielded no redshifts, all but one (which shows faint red continuum) have completely blank spectra, showing there is probably no contamination from lower-redshift ( $z \lesssim 1.4$ ) starbursts since they would have shown [OII] line emission, or if highly obscured, at least some continuum. We believe these blank-spectrum objects are also type-2 quasars with  $z \gtrsim 1.4$  and there is no compelling argument against them having  $z \gtrsim 2$  since the Lyman- $\alpha$  line can easily be extinguished if the host galaxy is dusty on large

(kpc) scales. We are probably seeing two types of type-2: the objects with narrow emission lines are obscured by the torus<sup>[3]</sup>, while the blank-spectrum objects are probably obscured by a starbursting host galaxy and we are seeing the coeval growth of supermassive black hole and host galaxy. Growing supermassive black holes embedded in a starburst have been found at  $z \sim 2$  from X-ray measurements of submillimetre-selected galaxies<sup>[21]</sup>.

To interpret our results in terms of the ‘quasar fraction’  $q$  – the ratio of the number of type-1 quasars to the total number of type-1 and type-2 quasars – we need to predict the average number  $\langle N_1 \rangle$  of type-1 quasars meeting identical  $S_{24\mu\text{m}}$  and  $S_{1.4\text{GHz}}$  selection criteria, and having matched redshift and sky area selection functions. We estimated a probability distribution  $p(\langle N_1 \rangle)$  to account for the various uncertainties, the gaussian approximation of which  $(4.3^{+2.2}_{-1.1})$  represents the expected number of type-1 quasars expected to adhere to both our  $24\text{-}\mu\text{m}$  and  $1.4\text{-GHz}$  selection criteria<sup>[22]</sup>, and with  $z \geq 2$  in a  $3.8 \text{ deg}^2$  patch; this number would be 15-times higher without any radio selection criteria.

FIG. 2 shows the resulting conditional probability distribution of the quasar fraction  $q$  given our new data on type-2 quasars and our background knowledge of the type-1 quasar population, namely  $p(q|\text{data}, \{\text{type-1 quasar}\})$ . This bayesian approach allows us to account properly for small number statistics (see FIG. 2 and Supplementary Information). It is difficult to judge whether the blank-spectrum objects with photometric redshifts  $z_{\text{phot}} > 2$  should be included (dashed red line in FIG. 2) until we know more about the dust content of their host galaxies, but considering just the objects with spectroscopic redshifts (solid blue line in FIG. 2) is clearly a conservative estimate.

The most likely systematic problem with our analysis is that we have implicitly assumed identical radio properties<sup>[22]</sup> for type-1 and type-2 quasars matched in intrinsic luminosity. However, ‘unified models’<sup>[3]</sup> predict Doppler-boosted radio emission from the weak jets aligned closer to the line-of-sight for type-1 quasars<sup>[23]</sup> and hence, on average, lower radio luminosities for type-2 quasars. This would yield lower derived values of  $q$  and strengthen our conclusion that most quasars are obscured. It is of course possible to postulate that the optical-to-radio correlation evolves with redshift, but this is currently an unknown (see also Supplementary Information).

The median redshift of our spectroscopic sample is at  $z = 2$  which is exactly where the optical luminosity density of the type-1 quasar population is at its peak<sup>[6]</sup>. Our sample shows that during this ‘epoch of quasar activity’ we can be confident that about half of all high-luminosity quasars are obscured and if some of the blank-spectrum objects turn out to have

$z \gtrsim 2$  then it is likely that type-2 quasars outnumber type-1 quasars by a significant factor. It is also possible that we are missing type-2 quasars with an extreme obscuring column ( $A_V \gtrsim 100$ ) which could be due, for example, to the obscuring torus being completely edge-on to the line of sight, but this would only strengthen our result, which has been predicted both by models for the X-ray background<sup>[1]</sup>, and by models predicting the surface density of faint AGN in relatively small sky area surveys<sup>[24]</sup>. This is, however, the first direct detection of a high-redshift type-2 quasar population likely to outnumber the type-1 population. We note that the solid blue line (which compares narrow-line or ‘torus-obsured’ type-2s with type-1s) is consistent with the quasar fraction from radio-loud samples<sup>[7]</sup>, while the dashed red line (which includes both ‘torus’ and ‘host-obsured’ type-2s) has enough obscured objects to account for the X-ray background<sup>[1]</sup>.

FIG. 2 shows the expected ratio for two ‘receding torus’<sup>[25,26,27]</sup> models in which the solid angle subtended by the obscuring torus decreases (so that  $q$  increases) systematically with increasing quasar luminosity. Since we have suggested that some of the blank-spectrum objects are obscured by kpc-scale dust, it is only the ratio of spectroscopically-confirmed type-2 quasars to type-1 quasars (the solid blue line) that is relevant to the model predictions, thus these models are not excluded.

To conclude, we consider our results alongside those of the X-ray surveys at lower redshifts<sup>[9]</sup> ( $z \lesssim 2$ ) which find that most accretion at low redshift occurs in type-2 quasars and type-2 Seyferts (their lower luminosity analogues). We deduce that throughout cosmic history, black hole growth seems to have been concentrated in obscured regions. This is in good agreement with predictions from the X-ray background<sup>[1]</sup> and implies, from comparisons between the integrated luminosity density of quasars (both type-1 and type-2) and the local space density of relic black holes<sup>[28]</sup>, that black hole growth occurs in short, efficient spurts in the cores of forming galaxies<sup>[2]</sup>.

**Received 24 December 2004; accepted 18 May 2005.**

---

[1] Worsley, M.A., Fabian, A.C., Barcons, X., Mateos, S., Hasinger, G., The (un)resolved X-ray background in the Lockman Hole, *Mon. Not. R. Astr. Soc.* **354**, 720-726 (2004)

[2] Fabian, A.C., The obscured growth of massive black holes, *Mon. Not. R. Astr. Soc.* **308**, L39-L43 (1999)

- [3] Antonucci, R., Unified models for active galactic nuclei and quasars, *Ann. Rev. Astron. Astrophys.* **31**, 473-521 (1993)
- [4] Rowan-Robinson, M., *et al.* A high-redshift IRAS galaxy with huge luminosity - Hidden quasar or protogalaxy? *Nature* **351**, 719-721 (1991)
- [5] Norman, C., *et al.*, A classic Type 2 quasar, *Astrophys. J.* **571**, 218-225 (2002)
- [6] Wolf, C., *et al.*, The evolution of faint AGN between  $z \sim 1$  and  $z \sim 5$  from the COMBO-17 survey, *Astron. Astrophys* **408**, 499-514 (2003)
- [7] Willott, C.J., Rawlings, S., Blundell, K.M., Lacy, M., The quasar fraction in low-frequency-selected complete samples and implications for unified schemes *Mon. Not. R. Astr. Soc.* **316**, 449-458 (2000)
- [8] Baker, J.C., *et al.*, Associated absorption in radio quasars. I. C IV absorption and the growth of radio sources, *Astrophys. J.* **568**, 592-609 (2002)
- [9] Barger, A.J., *et al.*, The Cosmic Evolution of Hard X-Ray-selected Active Galactic Nuclei, *Astron. J.* **129**, 578-609 (2005)
- [10] Zakamska, N.L., *et al.*, Candidate Type II Quasars from the SDSS: III. Spectropolarimetry Reveals Hidden Type I Nuclei, *Astron. J.* **129**, 1212-1224 (2005)
- [11] Zheng, W., *et al.*, Photometric redshifts of X-ray sources in the Chandra Deep Field South, *Astrophys. J. S.* **155**, 73-87 (2004)
- [12] Alexander, D.M., *et al.*, A Chandra observation of the  $z=2.285$  galaxy FSC10214+4724: Evidence for a Compton-thick quasar? *Mon. Not. R. Astr. Soc.* **357**, L16-L20 (2005)
- [13] Broadhurst, T., Lehar, J., A gravitational lens solution for the IRAS Galaxy FSC 10214+4724, *Astrophys. J.* **450**, L41-L44 (1995)
- [14] Serjeant, S., *et al.*, A spectroscopic study of IRAS F10214+4724, *Mon. Not. R. Astr. Soc.* **298**, 321-331 (1998)
- [15] Werner, M.W., *et al.*, The Spitzer Space Telescope Mission, *Astrophys. J. S.* **154**, 1-9 (2004)
- [16] Croom, S.M., *et al.*, The 2dF QSO Redshift Survey-XII. The spectroscopic catalogue and luminosity function, *Mon. Not. R. Astr. Soc.* **349**, 1397-1418 (2004)
- [17] Lacy, M., *et al.*, The Infrared Array Camera component of the Spitzer Space Telescope Extragalactic First Look Survey, *Accepted by Astrophys. J. S.* astro-ph/0507143
- [18] Condon, J.J., *et al.*, The SIRTF First-Look Survey. I. VLA Image and Source Catalog, *Astrophys. J.* **125**, 2411-2426 (2003)

- [19] Chapman, S.C., Blain, A.W., Smail, I., Ivison, R.J., A redshift survey of the submillimetre galaxy population, *Astrophys. J.* **622**, 772-796 (2005)
- [20] Rawlings, S., Eales, S., Warren, S., The detection of four high-redshift ( $0.5 \leq z \leq 3.22$ ) radiogalaxies by optical spectroscopy of five blank fields, *Mon. Not. R. Astr. Soc.* **243**, 14-18 (1990)
- [21] Alexander, D.M., *et al.*, Rapid Growth of Black Holes in Massive Star-Forming Galaxies, *Nature* **434**, 738-740 (2005)
- [22] Cirasuolo, M., Celotti, A., Magliocchetti, M., Danese, L., Is there a dichotomy in the radio loudness distribution of quasars? *Mon. Not. R. Astr. Soc.* **346**, 447-455 (2003)
- [23] Miller, P., Rawlings, S., Saunders, R., The Radio and Optical Properties of the  $z < 0.5$  BQS Quasars, *Mon. Not. R. Astr. Soc.* **263**, 425-460 (1993)
- [24] Treister, E., *et al.*, Obscured AGN and the X-ray, Optical and Far-Infrared Number Counts of AGN in the GOODS Fields, *Astrophys. J.* **616**, 123-135 (2004)
- [25] Lawrence, A., The relative frequency of broad-lined and narrow-lined active galactic nuclei – implications for unified schemes, *Mon. Not. R. Astr. Soc.* **252**, 586-592 (1991)
- [26] Simpson, C., A new look at the isotropy of narrow-line emission in extragalactic radio sources, *Mon. Not. R. Astr. Soc.* **297**, L39-L43 (1998)
- [27] Simpson, C., The luminosity dependence of the type 1 active galactic nucleus fraction, *Mon. Not. R. Astr. Soc.* **360**, 565-572 (2005)
- [28] Yu, Q., Tremaine, S., Observational constraints on growth of massive black holes, *Mon. Not. R. Astr. Soc.* **335**, 965-976 (2002)
- [29] Marleau, F.R., *et al.*, Extragalactic Source Counts at 24 Microns in the Spitzer First Look Survey, *Astrophys. J. S.*, **154**, 66-69 (2004)
- [30] Bruzual, G., Charlot, S., Stellar population synthesis at the resolution of 2003, *Mon. Not. R. Astr. Soc.* **344**, 1000-1028 (2003)
- [31] Rowan-Robinson, M., A new model for the infrared emission of quasars, *Mon. Not. R. Astr. Soc.* **272**, 737-748 (1995)
- [32] Pei, Y.C., Interstellar dust from the Milky Way to the Magellanic Clouds, *Astrophys. J.* **395**, 130-139 (1992)

---

**Supplementary Information** is linked to the online version of the paper at [www.nature.com/nature](http://www.nature.com/nature).

**Acknowledgments.** A.M.-S. is grateful to the Council of the European Union for finan-

Name	RA (J2000)	Dec	$S_{24\mu\text{m}}$ / $\mu\text{Jy}$	$S_{1.4\text{GHz}}$ / $\mu\text{Jy}$	$S_{3.6\mu\text{m}}$ / $\mu\text{Jy}$	$S_{4.5\mu\text{m}}$ / $\mu\text{Jy}$	$z_{\text{phot}}$	$z_{\text{spec}}$	Comments on Spectroscopy
AMS01	17 13 11.17	+59 55 51.5	536	490	25.0	30.0	2.1		Blank
AMS02	17 13 15.88	+60 02 34.2	294	1184	44.5	61.0	1.4		Blank
AMS03	17 13 40.19	+59 27 45.8	500	1986	16.0	28.0	3.1	2.689	Single line <sup>†</sup>
AMS04	17 13 40.62	+59 49 17.1	828	536	18.0	22.0	2.8	1.782	
AMS05	17 13 42.77	+59 39 20.2	1769	1038	34.7	61.4	1.7	2.022	Weak Lyman- $\alpha$
AMS06	17 13 43.91	+59 57 14.6	969	444	<20	<25	$\geq 2.5$		Blank
AMS07	17 14 02.25	+59 48 28.8	503	354	37.9	47.8	1.5		Blank
AMS08	17 14 29.67	+59 32 33.5	792	655	41.6	46.3	1.4	1.979	
AMS09	17 14 34.87	+58 56 46.4	685	426	25.2	<25	2.1		Blank
AMS10	17 16 20.08	+59 40 26.5	338	1645	39.2	44.7	1.5		Blank
AMS11	17 18 21.33	+59 40 27.1	442	356	32.4	55.6	1.7		Blank
AMS12	17 18 22.65	+59 01 54.3	518	946	25.24	<25	2.0	2.770	
AMS13	17 18 44.40	+59 20 00.8	4196	1888	24.7	49.1	2.1	1.986	
AMS14	17 18 45.47	+58 51 22.5	937	469	8.0	15.0	4.6	1.504	
AMS15	17 18 56.93	+59 03 24.1	371	440	16.0	16.0	3.0		Blank
AMS16	17 19 42.07	+58 47 08.9	788	390	18.0	21.0	2.8	4.174	
AMS17	17 20 45.17	+58 52 21.3	1134	615	10.0	15.0	3.9	3.138	Single line <sup>†</sup>
AMS18	17 20 46.32	+60 02 29.6	925	390	<20	<25	$\geq 2.5$	1.418	
AMS19	17 20 48.00	+59 43 20.7	1433	822	<20	26.9	$\geq 2.5$		Blank
AMS20	17 20 59.10	+59 17 50.5	492	1268	45.2	64.9	1.4		Faint Red Continuum
AMS21	17 21 20.09	+59 03 48.6	720	449	25.2	38.6	2.1		Blank

**Table 1.** Basic data on the 21 type-2 quasars in our sample. The J2000.0 positions are from the Spitzer FLS radio catalogue<sup>[18]</sup>. RA, right ascension, Dec., declination. The MIPS 24- $\mu\text{m}$  flux density  $S_{24\mu\text{m}}$  is obtained by point spread function (PSF) fitting<sup>[29]</sup> as all objects are point sources at the  $\sim 6$  arcsecond resolution of the MIPS observations, with positional errors  $\sim 1$  arcsecond. It has a typical error of  $\pm 10 - 15$  per cent. The 1.4-GHz flux density is the peak value (in  $\mu\text{Jy}$  per beam) from the radio catalogue<sup>[18]</sup>. The IRAC 3.6- and 4.5- $\mu\text{m}$  flux densities are measured in 5-arcsec-diameter apertures<sup>[17]</sup> and have typical errors of  $\pm 10$  per cent. The photometric redshifts are calculated by assuming that the 3.6- $\mu\text{m}$  flux density is dominated by starlight from a  $2L_{\text{gal}}^*$  galaxy ( $L_{\text{gal}}^*$  is the break in the galaxy luminosity function, following the models of ref.<sup>[30]</sup> and passive evolution). The criterion  $S_{3.6\mu\text{m}} \leq 45 \mu\text{Jy}$  corresponds to a limiting photometric redshift  $z_{\text{phot}} \geq 1.4$ ; this was chosen to allow for scatter in the photometric redshift estimation, whilst still filtering out type-1 quasars and low-redshift contaminants like radio galaxies. All of the 21 candidates were observed spectroscopically with the dual-beam ISIS instrument at the William Herschel Telescope, on July 2004 and April 2005. ‘Blind’ low-resolution spectroscopy<sup>[20]</sup> was performed by offsetting from nearby stars to the radio positions, with exposure times of  $\sim 30$  minutes and a continuous wavelength coverage across the entire visible band. Objects with a<sup>†</sup> have only one definite line in their optical spectra, which is taken to be Ly- $\alpha$  by virtue of extreme equivalent width, blue-absorbed line profile and lack of other lines supportive of alternative identifications.

cial support. S.R. and C.S. are grateful to the UK PPARC for a Senior Research Fellowship and an Advanced Fellowship respectively. We thank C. Wolf, L. Clewley, H.-R. Klöckner, and G. Cotter for useful discussions, and the referees for valuable comments.

**Author Information.** Reprints and permissions information is available at [npg.nature.com/reprintsandpermissions](http://npg.nature.com/reprintsandpermissions). The authors declare no competing financial interests. Correspondence and requests for material should be addressed to A.M.-S. (email: a.martinez-sansigre1@physics.oxford.ac.uk).

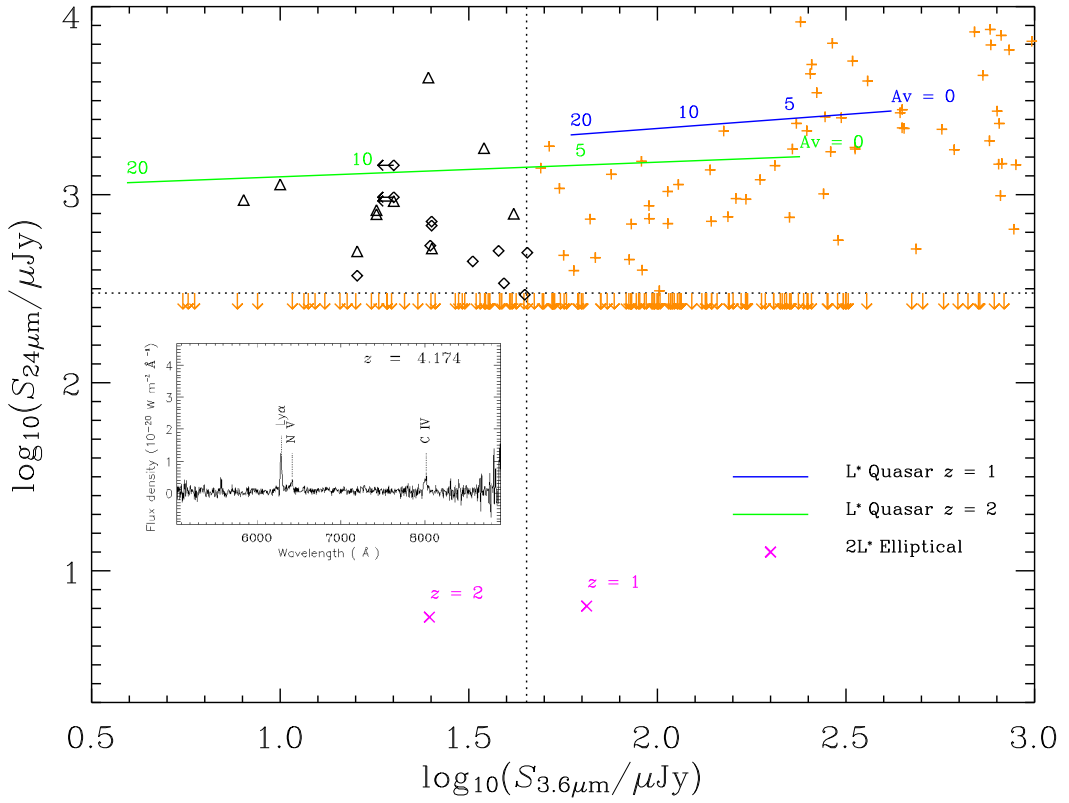


**Figure 1.** Diagrammatic representation of the infrared selection criteria.  $\log_{10}(24 \mu\text{m} \text{ flux density } S_{24\mu\text{m}} / \mu\text{Jy})$  plotted against  $\log_{10}(3.6 \mu\text{m} \text{ flux density } S_{3.6\mu\text{m}} / \mu\text{Jy})$ . The dotted lines represent the flux density cuts of our selection criteria. Note that all objects plotted needed to meet the criteria on radio flux density described in the text, and that the candidates were originally selected from the preliminary 3.6 and 24  $\mu\text{m}$  catalogues, but have had their fluxes slightly revised. This explains why two candidates are slightly outside the selection boundaries (see Supplementary Information). The parent population is plotted as orange crosses, or arrows when  $S_{24\mu\text{m}}$  is an upper limit. Our 21 candidates are plotted in the top left corner, with black triangles for candidates with a spectroscopic redshift and black diamonds for candidates without one. Horizontal arrows represent upper limits for  $S_{3.6\mu\text{m}}$ . None of the candidates showed type-1 quasar spectra. The spectrum of the  $z = 4.174$  object is shown in the inset. The magenta crosses show  $S_{24\mu\text{m}}$  and  $S_{3.6\mu\text{m}}$  for a  $2L_{\text{gal}}^*$  elliptical galaxy at  $z = 1$  and  $z = 2$ ; starlight is assumed to evolve passively following a stellar population synthesis model<sup>[30]</sup>. The other colours represent an  $L_{\text{quasar}}^*$  quasar (spectral energy distribution from ref<sup>[31]</sup>) with varying amounts of visual extinction  $A_V$  applied to  $S_{24\mu\text{m}}$  and  $S_{3.6\mu\text{m}}$  and plotted on the curves (assuming a Milky-Way-like extinction curve from ref<sup>[32]</sup>); these are plotted at two different redshifts, and the quasar population is assumed to undergo pure luminosity evolution<sup>[16]</sup>. At all redshifts, any type-1 ( $A_V = 0$ ) quasar bright enough to make the  $S_{24\mu\text{m}} > 300 \mu\text{Jy}$  criterion will also be too bright at 3.6- $\mu\text{m}$  to make it into our sample. Inset, the optical spectrum of AMS16, showing Lyman- $\alpha$ , N V and C IV emission lines.

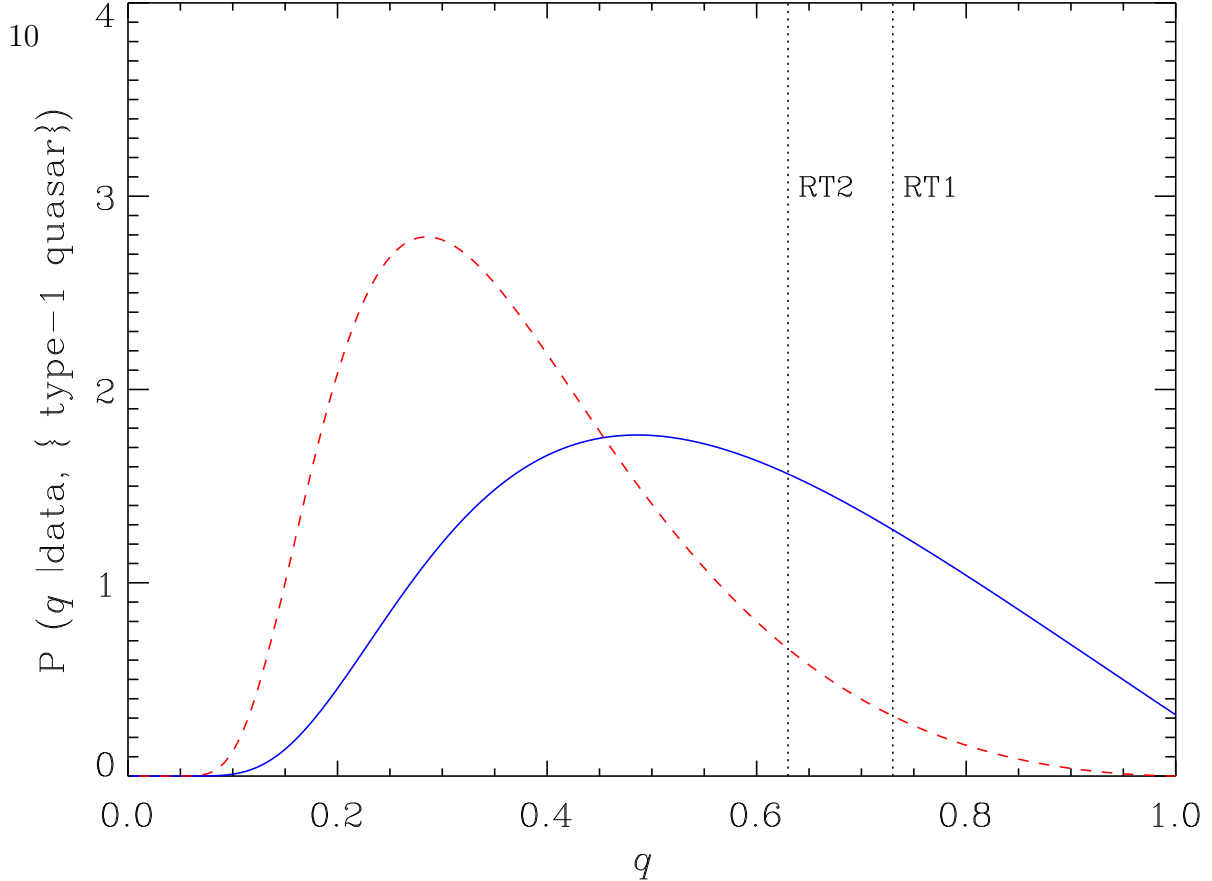


**Figure 2.** Probability distributions for the quasar fraction. The normalised posterior probability  $p(q|\text{data}, \{\text{type-1 quasar}\})$  of the quasar fraction  $q$  given our new data on type-2 quasars, and background information on type-1 quasars. The two lines represent different interpretations of the number of type-2 quasars at  $z \geq 2$  determined from our new data. To obtain  $p(q|\text{data}, \{\text{type-1 quasar}\})$  we used Bayes' theorem with a uniform prior over the range  $0 \leq q \leq 1$  so that the  $p(q|\text{data}, \{\text{type-1 quasar}\}) = p(\text{data}|q, \{\text{type-1 quasar}\})$ . We then calculated this likelihood function, at each  $q$ , as a Poisson distribution for the observed (integer) number of type-2 quasars at  $z \geq 2$  where the mean number expected  $\langle N_2 \rangle = (1 - q) \langle N_1 \rangle / q$ . Because of uncertainties in the background information on  $\langle N_1 \rangle$ , we had to evaluate the likelihood at each  $q$  and  $\langle N_1 \rangle$  and then integrate  $p(\langle N_1 \rangle) \times$  the likelihood over  $\langle N_1 \rangle$ . The solid blue line is the posterior probability if we believe the only candidates with  $z \geq 2$  are the 5 whose spectroscopic redshifts confirm this. If, additionally, we use the photometric redshifts of the candidates with blank spectra (6 additional candidates with  $z \geq 2$ ), then we obtain the red curve. The best estimate for  $q$  is probably somewhere between the two curves. The two vertical lines represent the predictions of receding torus models, one with a fixed torus height (marked 'RT1')<sup>[26]</sup> and one ('RT2') with a torus height varying with luminosity<sup>[27]</sup>.